Electron Doping by Charge Transfer at $LaFeO_3/Sm_2CuO_4$ Epitaxial Interfaces

Flavio Y. Bruno, Rainer Schmidt, Maria Varela, Javier Garcia-Barriocanal, Alberto Rivera-Calzada, Fabian A. Cuellar, Carlos Leon, Pardeep Thakur, Julio C. Cezar, Nicholas B. Brookes, Mar Garcia-Hernandez, Elbio Dagotto, Stephen J. Pennycook, and Jacobo Santamaria**

The breakdown of the lattice translational invariance symmetry that occurs at complex oxide interfaces may profoundly modify their electronic structure, leading to interfacial states with properties drastically different from those of the superlattice individual components. The appearance of a conducting two dimensional (2D) electron gas at the interface between two insulating oxides and induced magnetism in a non-magnetic material are just two among many fascinating examples.[1–8] One of the key factors underlying novel properties is the modification of the doping and orbital occupancy near those interfaces, which may result from charge transfer processes.[3,9–11] If materials used in heterostructures have different work functions, a non-equilibrium situation will be created at the interface and charge will be transferred until the chemical potential levels off.[12] The use of such phenomena to modify doping in heterostructures has been proposed theoretically as a new route to avoid the quenched disorder that inevitably accompanies the chemical doping. At the interface between a Mott insulating parent compound of the high critical temperature superconductor (HTSC) family and a suitable material that would act as the charge donor, electron doped phases could be stabilized which would eventually turn metallic and perhaps superconducting.[12,13] Such charge transfer processes have been observed at interfaces involving copper oxides such as $La_{0.7}Ca_{0.3}MnO_3/YBa_2Cu_3O_7$,[14] $La_{2-x}Sr_xCuO_4/La_2CuO_4$[15] and $SrTi_{1-x}Nb_xO_3/Sm_2CuO_4$.[16] While a novel 2D superconducting state was found at the $La_{2-x}Sr_xCuO_4/La_2CuO_4$ interface,[17] the effect of doping by charge transfer could not be examined in the other two cases due to the detrimental effect on the $YBa_2Cu_3O_7$ superconductivity of the spin polarized electrons from $La_{0.7}Ca_{0.3}MnO_3$ in one case and due to the conducting nature of the $SrTi_{1-x}Nb_xO_3$ in the other case, which obscures changes in the conducting properties of the interface layer.

In this paper, the structural and electronic properties of heterostructures involving Sm_2CuO_4 (SCO) and $LaFeO_3$ (LFO) will be studied. SCO is a Mott insulator that becomes superconducting upon replacing Sm^{3+} ions with Ce^{4+} to form $Sm_{2-x}Ce_xCuO_4$, an electron doped HTSC.[18] LFO is also a Mott insulator with its chemical potential being approximately 1 eV above the chemical potential of SCO.[12,19,20] The gap in both of these materials is of the charge-transfer (CT) type, i.e. the energy difference Δ between the O–2p band and the upper Hubbard band is smaller than the energy difference U between the lower and upper Hubbard bands.[21] The transfer of charge involving CT Mott insulators provides an interesting framework, which to our knowledge has not been examined before. Moreover, LFO is a good candidate to transfer electrons from its O 2p valence band to the CuO_2 d-like upper Hubbard band of the SCO. Since $La_{1-x}Sr_xFeO_3$ remains insulating and antiferromagnetic even if doped with holes up to $x < 0.7$, this state should not be detrimental to a possible superconducting state if an interface with SCO is made.[22] Here, it will be shown that it is indeed possible to obtain a doped n-type material at the SCO/LFO interface of two CT insulators, which displays metallic behavior in the temperature range of 150–300 K.

We have grown superlattices consisting of six bilayers of 14 unit cells (u.c.) of LFO and N u.c. SCO ($[LFO_{14}/SCO_N]_6$) on TiO_2 terminated (001) $SrTiO_3$ (STO) substrates[23] in a high-pressure pure oxygen sputtering system. Thin films of LFO and SCO were also grown as control samples. The lattice parameter of STO is 0.391 nm which imposes a lattice mismatch of –0.1% and –0.5% for LFO and SCO respectively. SCO has the Nd_2CuO_4 (abbreviated T′) structure with lattice constants a = 0.3914 nm and c = 1.197 nm. The T′ structure is composed of sheets of CuO_2 squares with no apical oxygens as shown in

Dr. F. Y. Bruno, Dr. R. Schmidt, Dr. M. Varela, Dr. J. Garcia-Barriocanal, Dr. A. Rivera-Calzada, Dr. F. A. Cuellar, Dr. C. Leon, Prof. J. Santamaria
GFMC. Dpto. Física Aplicada III
Universidad Complutense de Madrid
Campus Moncloa, Madrid, 28040, Spain
E-mail: flavioyb@fis.ucm.es; jacsan@fis.ucm.es
Dr. M. Varela, Dr. E. Dagotto, Dr. S. J. Pennycook
Materials Science and Technology Division
Oak Ridge National Laboratory
Oak Ridge, Tennessee 37831-6071, USA
Dr. P. Thakur, Dr. J. C. Cezar, Dr. N. B. Brookes
European Synchrotron Radiation Facility (ESRF)
6 rue Jules Horowitz, B.P. 220, Grenoble Cedex 38043, France
Dr. M. Garcia-Hernandez
Instituto de Ciencia de Materiales de Madrid
Consejo Superior de Investigaciones Cientificas
Cantoblanco 28049, Spain
Dr. E. Dagotto
Department of Physics and Astronomy
University of Tennessee
Knoxville, Tennessee 37996, USA

DOI: 10.1002/adma.201203483

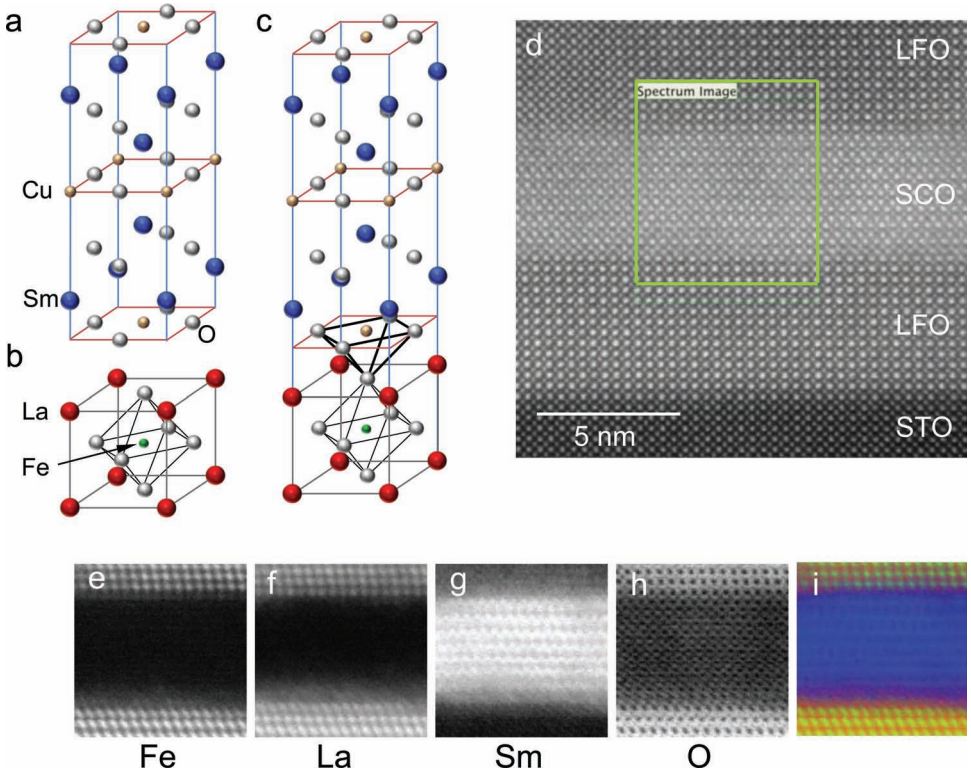

Figure 1. Crystal structure of (a) Sm_2CuO_4 (T'-phase), (b) pseudocubic representation of $LaFeO_3$, and (c) interface formed by these compounds. In (c) the interfacial Cu-O pyramid is highlighted. (d) High-resolution scanning transmission electron microscopy image of a $[LFO_{14}/SCO_4]_6$ heterostructure. EELS elemental maps using normalized integrated intensities for the (e) Fe $L_{2,3}$, (f) La $M_{4,5}$, (g) Sm $M_{4,5}$ and (h) O K absorption edges. The color map of panel (i) has been produced by overlaying the Sm image (blue), Fe image (green), and the La image (red).

Figure 1a. The orthoferrite LFO is an insulating antiferromagnetic material with orthorhombic Pbnm structure and lattice parameters a = 0.555, b = 0.556 and c = 0.787 nm. The LFO unit cell is composed of distorted perovskite blocks with lattice parameter $a^* = 0.393$ nm as shown in Figure 1b.

Figure 1d displays an atomic resolution high angle annular dark field (ADF) scanning transmission electron microscopy image (also known as Z-contrast) of a $[LFO_{14}/SCO_4]_6$ superlattice. Good epitaxial properties and coherent growth are observed in the LFO/STO substrate interface, as well as at the interface formed by SCO and LFO. This is consistent with having fully strained heterostructures, as demonstrated by X-ray diffraction experiments (see Supporting Information). Figures 1e-h show elemental maps corresponding to the Fe $L_{2,3}$, La $M_{4,5}$, Sm $M_{4,5}$ and O K absorption edges. These have been obtained by integrating the intensities under the edges after background subtraction using a power law. Principal component analysis was used to remove random noise. Both the FeO_2 and the LaO atomic planes can be resolved from each other in the chemical images, and a direct count shows that both the top and bottom interfaces are LaO terminated (Figure 1e and 1f). In the combined elemental maps of Figure 1i, there is a La (red) atomic layer at the interface and no Fe (green) atomic planes are observed. These observations prove that the LFO layer terminates on a LaO plane at both interfaces. The atomic plane observed between the Sm (blue) and the LaO atomic plane in Figure 1i belongs, therefore, to the cuprate and it is a CuO_2 plane. Thus the atomic plane stacking at the interface is Sm-CuO_2-LaO as shown in the schematic of Figure 1c. The top and bottom interfaces are symmetrical as has been found before in heterostructures grown by sputtering.[24]

In the ionic limit, the formal valence states in the SCO compound are Sm^{3+}, Cu^{2+} and O^{2-}. When doping with a tetravalent cation like Ce^{4+}, electrons are added to the CuO_2 planes which implies a mixed Cu^{2+}/Cu^{1+} oxidation state. In order to establish the oxidation state of the Cu atoms at the SCO/LFO interfaces electron energy loss spectroscopy (EELS) measurements have been performed. In cuprates it is well established that the carrier density is related to the occupancy of the oxygen 2p bands, as obtained from the oxygen absorption spectra.[25,26] **Figure 2**a shows the reference spectra for the oxygen K-edge for two bulk samples, Sm_2CuO_4 and the optimally doped superconductor $Sm_{1.84}Ce_{0.16}CuO_4$ (SCCO). Clear differences in the spectral features can be observed. We also acquired EEL spectra across a $[LFO_{14}/SCO_4]_6$ superlattice. To study quantitatively the electron doping at the interfaces and SCO layers we performed a multiple linear least square (MLLS) fit of the O K edge in the superlattice to the reference spectra. The coefficients in the MLLS fit corresponding to SCO and SCCO are C_N and C_S respectively. With this approach we have a quantitative measure of how similar the O K edge spectrum in the superlattice is to the O K edge in SCCO. The MLLS coefficients are shown in

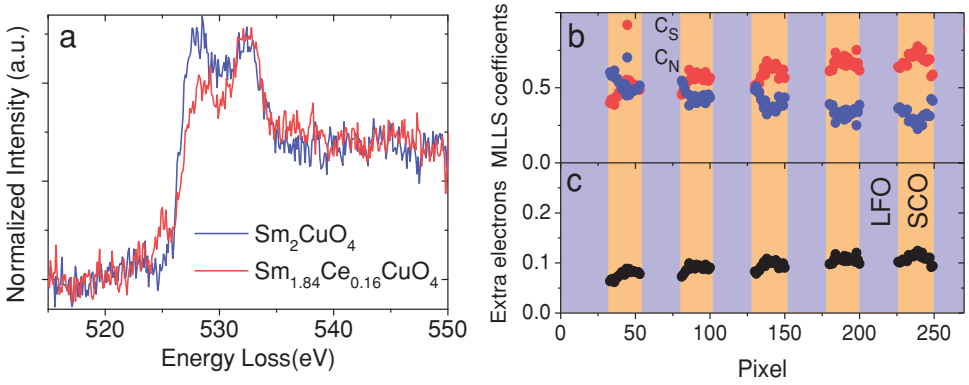

Figure 2. (a) Reference EELS spectra of the O K absorption edge taken from powder samples of Sm_2CuO_4 (blue) and $Sm_{1.84}Ce_{0.16}CuO_4$ (red). (b) MLLS coefficients and (c) extra electrons per formula unit for the $[LFO_{14}/SCO_4]_6$ heterostructure.

Figure 2b. Since we know that in SCCO there are 0.16 extra electrons per Cu atom when compared with the undoped case (SCO), the amount of extra electrons in the heterostructure can be obtained by multiplying Cs by 0.16. Figure 2c shows the excess of electrons in the cuprate layers, with a mean value of 0.09+/−0.01 per formula unit. This analysis demonstrates an excess of electrons in the SCO layers which cannot be explained through chemical doping.

To probe directly the oxidation state of Cu we have performed X-ray absorption spectroscopy (XAS) measurements with synchrotron radiation. The cuprates are highly anisotropic materials and insight into its electronic structure can be gained by performing XAS experiments with polarized light. In these regards it is very important to recall that orbital occupation at the interface may be drastically modified,[27] and as was shown in the case of $La_{0.7}Ca_{0.3}MnO_3/YBa_2Cu_3O_7$[9] and $LaMnO_3/SrTiO_3$[28,29] orbital reconstruction and covalent bonding at the interface may play an important role in determining the characteristics of the charge transfer process. In **Figures 3**a and b we show a Cu L_3 absorption spectrum normalized to the edge jump obtained with horizontal (H) and vertical (V) polarized light, respectively, for both the control sample consisting of a thin film 15 u.c. thick of SCO (red) and a $[LFO_{14}/SCO_2]_6$ superlattice (blue). In the insets of Figure 3a and b we show schematics of the experimental setup to measure the XAS spectra with H and V-polarized photons. In the case of V-polarization the electric field is parallel to the surface sample and, in consequence, parallel to the **ab** plane (CuO_2 planes), while in the case of the H-polarization the electric field has components perpendicular and parallel to the film plane. Because the incidence angle of the photons is $\alpha = 30°$ measured from the film surface plane, most of the E field intensity ($\cos^2(30) = 0.75$) will be parallel to **c** the surface normal in the case of H-polarization. Thus, H and V-polarization probe out of plane and in plane orbital states respectively. The main peak $L_3 \approx 932{,}8$ eV observed in the spectra is associated with transitions in formally divalent copper states from the Cu^{2+} ground state $3d^9$ to the $\underline{2}_{p3/2}3d^{10}$ excited state,where $\underline{2}_{p3/2}$ denotes a $2_{p3/2}$ hole.[30,31] The second common feature only observed in spectra obtained with H polarized light is the broad peak at 938.4 eV, which is associated with a transition in Cu^{2+} to the excited state $\underline{2}_{p3/2}3d^94s^1$.[30,32] However the main difference between the spectra of both samples is the presence of the 935.6 eV peak associated with the presence of Cu^{1+} clearly visible for the superlattice with H and V polarized light. Nevertheless, in the case of H polarization the associated peak is clearly more intense, indicating the out of plane character of these states. These features are observed in the Cu 2p excitation spectra of cuprates due to hybridization

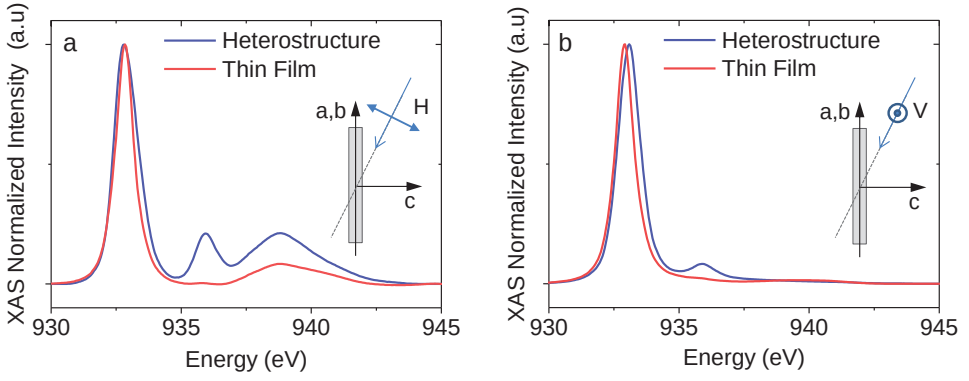

Figure 3. X-ray absorption spectra obtained with (a) horizontal and (b) vertical polarization. The spectra correspond to a $[LFO_{14}/SCO_2]_6$ superlattice (blue) and a SCO 15 u.c. thick film (red). (Inset) schematics of the experimental setup.

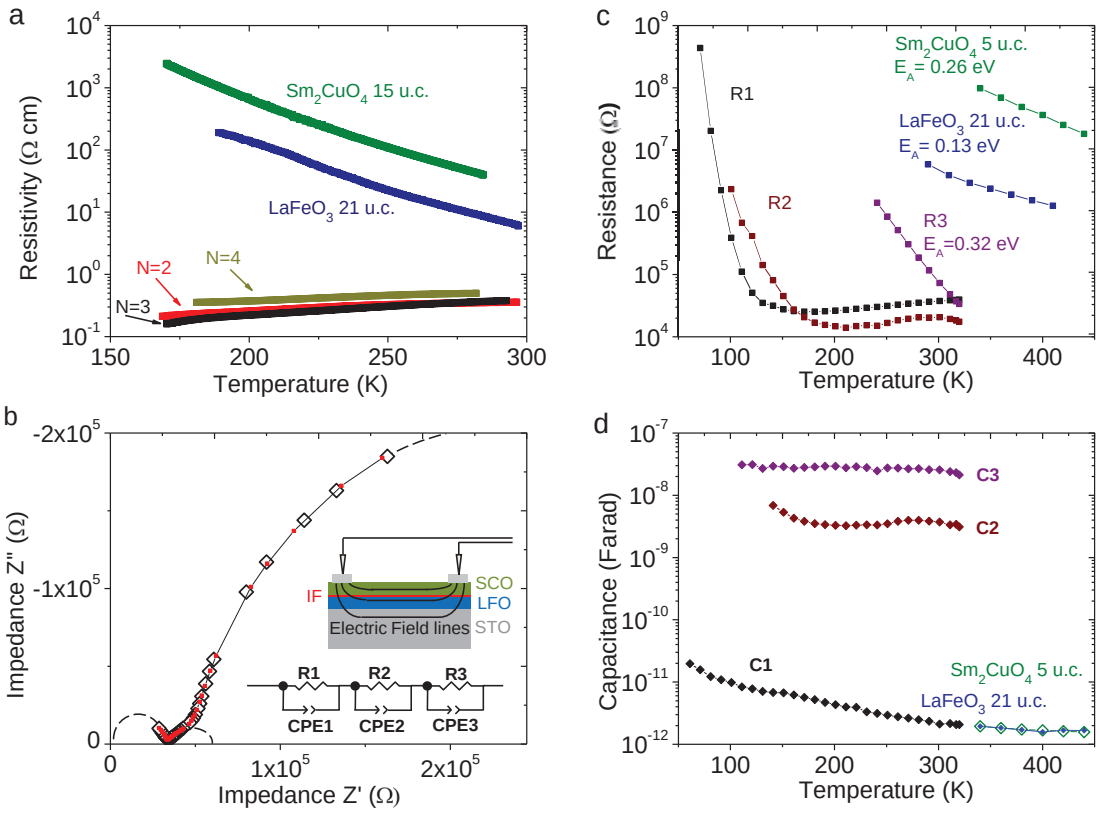

Figure 4. (a) Resistivity as a function of temperature of $[LFO_{14}/SCO_N]_6$ heterostructures, LFO_{21} and SCO_{15} thin films. (b) Impedance spectroscopy measurement of $[LFO_{14}/SCO_2]_6$ at T = 260 K. Open symbols represent data points, red solid squares and thin solid lines represent fits using the model shown in the lower figure inset. (c) Resistor and (d) capacitor values used to model the relaxation processes of $[LFO_{14}/SCO_2]_6$. The resistance and capacitance measurements on LFO_{21} and SCO_5 control samples are also included.

of the Cu^{1+} $3d_{3z2\text{-}r2}$ and apical O $2p_z$ orbitals.[33–35] In the case of the superlattice the Cu atoms in the interfacial CuO_2 planes have apical oxygens as shown in Figure 1c whilst it is known that there are no apical oxygens in bulk SCO. This provides evidence for the existence of a Cu^{1+} $3d_{3z2\text{-}r2}$ - apical O $2p_z$ bond resulting from an orbital reconstruction at the interfacial plane.

The transport properties of the aforementioned samples have also been examined. The temperature dependent direct current (dc) resistivity of $[LFO_{14}/SCO_N]_6$ is displayed in **Figure 4**a with N = 4 (red), 3 (black) and 2 (brown), measured in Van der Pauw configuration. The SCO/LFO superlattices show metallic-like behavior (dR/dT > 0) in the temperature range 300–170 K. The resistivity of bulk n-type cuprates is often modeled as $\rho = \rho_o + AT^M$, where $M = 2$ for optimally-doped superconducting samples and $1 < M < 1.5$ for the underdoped case.[36] In our heterostructures it was found that $M = 1.5$, 1, and 1.1 for superlattices with 4, 3, and 2 u.c. of SCO, evidencing that the metallic resistivity originates in the SCO layers and that the doping level of the cuprate layers is in the range $0.05 < x < 0.1$. In all measured superlattices it was impossible to obtain the resistance in the Van der Pauw configuration below 170 K because of the difficulty in injecting current through the large contact resistance. The sheet carrier density of $[LFO_{14}/SCO_4]_6$ measured in Van der Pauw Hall geometry at room temperature is $n_s = 1.5 \times 10^{13}$ cm^{-2} with electron-like carriers as expected. This carrier density is not far from what is found in other conducting interfaces like $LaAlO_3/SrTiO_3$. However in contrast to that case where the carrier density is constant or slightly increased at 200 K, here as the temperature is lowered the carrier density decreases to $n_s = 6.8 \times 10^{12}$ cm^{-2} showing that conduction mechanisms in both systems are different.[37] Considering that the carriers are confined to 0.5 nm from the interface we calculate that the carrier density in SCO will be $n = 2 \times 10^{19}$ cm^{-3}, far too low to obtain superconductivity but enough to obtain a metallic behavior in an underdoped cuprate.[38] As expected, the resistance of LFO_{21} and SCO_{15} thin films, grown in the same conditions as the superlattices, increases when lowering the temperature compatible with its insulating character. Resistance measurements made with different contacting methods (see supporting information) consistently showed that the induced interfacial state has metallic properties from 300 K down to at least 170 K. To circumvent the problem of the contact resistance in our samples we examined the transport properties using dielectric spectroscopy. Impedance Spectroscopy (IS) data collected for a $[LFO_{14}/SCO_2]_6$ multilayer sample at 260 K are shown in Figure 4b in the form of a complex impedance plane plot of $-Z'$ vs Z'. A sketch of the measurement set-up is displayed in the inset, which also schematically indicates the electric field lines. The three semicircles displayed in the $-Z''$ vs Z' plots are consistent with a series connection of 3 conventional dielectric relaxation processes, which

we modeled by a series of three parallel resistor-capacitor (RC) elements (see lower figure inset).[39,40] Not all three semicircles are fully developed and show considerable overlap, which is highlighted by the dotted model semicircles. Notice that the semicircle centre seems to be slightly depressed below the Z' x-axis indicating a certain degree of non-ideality of the relaxation process, which can be modeled with a constant phase element (CPE)[40] (see also the Supporting Information). This non ideal circuit model produced a good fit at all frequencies. Figure 4c displays the temperature dependence of all 3 resistor values for the multilayer sample obtained from the fitting procedures, together with the resistance values of the single phase LFO and SCO control samples. The dielectric spectra of the control samples exhibited single intrinsic film dielectric relaxations, and the resistance values were obtained from fits using one simple R-CPE circuit. The three dielectric relaxations displayed were associated with an insulating contribution from the electrode/surface sample interface (R3-CPE3) and two conducting contributions from the LFO/SCO interface (R1-CPE1, R2-CPE2). The resistance of the multilayer is drastically reduced as compared to the control samples (see Figure 4c), and displays metallic behavior in the temperature range $T > 120$–170 K. This supports the previous experimental evidence and indicates the n-doping of the SCO due to charge transfer. The much smaller values of the C1 capacitance as compared to C2 and C3 (see Figure 4d) supports the assignment that the R1-CPE1 relaxation process reflects transport parallel to the layers (in-plane), whereas the high conductivity of R1 as compared to the control samples most likely implies that charge transport occurs mainly near the doped interface. On the other hand, R2-CPE2 and R3-CPE3 are related to perpendicular transport and electrode processes respectively (See supporting information section for details). The metallic behavior in a limited temperature range and subsequent upturn below 120 K exhibited by the R1 circuit element is thus ascribed to a metal insulator transition occurring in the doped layer. This behavior is found in strongly underdoped (non superconducting) electronic cuprates,[36] which, according to the phase diagram, suggests a level of doping at our interfaces in the range $0.05 < x < 0.14$, which is insufficient to make the sample superconducting but agrees well with the doping level of 0.09+/−0.01 per formula unit determined from the EELS measurements mentioned above.

To summarize, we have realized electron doping by charge transfer in superlattices of SCO/LFO, i.e. between Mott insulators with a charge-transfer type gap as expected from the band alignment of these materials. High resolution EELS measurements at the O-K edge have provided evidence for 0.09+/−0.01 extra electrons per formula unit in the SCO *d*-band as revealed by a reduction of the Cu oxidation state. The transfer of electrons from LFO to SCO is further supported by the spectroscopic signature of Cu^{1+} obtained from XAS measurements. Transport measurements provide evidence of a metallic state at the interface between two nominally insulating materials. Dielectric spectroscopy measurements have allowed us to assign the metallic state to the LFO/SCO interfaces, consistent with DC measurements. When lowering the temperature a metal to insulator transition occurs at 120 K, indicating, in accordance with the phase diagram, an insufficient doping level to enter the superconducting state of SCO. Theoretical work is also necessary to establish the possible influence of the bonding between the Cu $3d_{3z2\text{-}r2}$ and apical O $2p_z$ orbitals at the interface in the absence of superconductivity observed here.

Experimental Section

All samples have been grown in a high pressure pure oxygen sputtering system. We deposited the LFO films at 800 °C and the SCO films at 650 °C, when growing the superlattices the substrate temperature was modified after the deposition of each layer. Oxygen pressure during growth was $P_{O2} = 2.8$ mbar, after the deposition samples were annealed during 10 min at 750 °C under an oxygen pressure of 900 mbar before cooling to room temperature at a rate of 20 °C/min.

X-ray absorption experiments were carried out at beam line ID08 of the ESRF where we have measured the Cu L-edge absorption spectra in total electron yield mode. STEM-EELS observations were carried out in a Nion UltraSTEM equipped with a spherical aberration correction and a Gatan Enfina EEL spectrometer, operated at 100 kV. Specimens were prepared by conventional methods: mechanical thinning and ion milling.

Direct current transport measurements of heterostructures were made in standard Van der Pauw configuration (four points measurement). Electrical contacts to the samples have been made by evaporating Ag spots. For dielectric measurements the samples were placed on a custom built probe, which can fit into a Quantum Design PPMS measurement system providing variable magnetic fields (up to 14 Tesla) and variable temperature (1.7–320 K). The custom built probe was necessary in order to minimize the internal probe capacitance (≈0.2 pF) and maximize the internal probe resistance (≈10 GΩ), which are both detrimental for reliable alternating current (ac) dielectric measurements. The sample tray at the bottom of the probe was equipped with 2 spring loaded drop down pins in order to ensure optimal contact between the pins and the Ag electrodes on the film surfaces. A QuadTech impedance analyzer was used for two-point dielectric spectroscopy measurements with an applied alternating voltage amplitude of 20 mV operating between 20 Hz–1 MHz. Data were collected in the form of the real and imaginary parts of the impedance (Z'–Z'') between 10 K–320 K. The LFO and SCO control samples showed high resistance, which could be resolved only at higher temperature. Therefore, dielectric spectroscopy measurements were carried out between 340 K–440 K using a Novocontrol Alpha-A High Performance Frequency Analyzer employing a 100 mV amplitude alternating voltage signal. Data was obtained in terms of the real and imaginary parts of the impedance (Z'–Z'') between 1 Hz–3 MHz. Equivalent circuit fitting for all dielectric data sets was performed using commercial software (Z-View) employing a least-linear square fitting routine of the real and imaginary parts of the data simultaneously.

Supporting Information

Supporting Information is available from the Wiley Online Library or from the author.

Acknowledgements

Work at UCM supported by Spanish MICINN Grant MAT 2011 27470, Consolider Ingenio CSD2009-00013 (IMAGINE), CAM S2009-MAT 1756 (PHAMA) and ERC starting Investigator Award, grant #239739 STEMOX. The authors thank Masashi Watanabe for the Digital Micrograph PCA plug-in and Julia Luck for help with specimen preparation. Research at ORNL (SJP, MV and ED) was sponsored by the U.S. Department of Energy, Basic Energy Sciences, Materials Sciences and Engineering Division. R.S. wishes to acknowledge the Ministerio de Ciencia e Innovacion (MICINN) for granting a Ramon y Cajal Fellowship. We

acknowledge the European Synchrotron Radiation Facility for provision of synchrotron radiation facilities.

Received: August 21, 2012
Revised: October 23, 2012
Published online: January 4, 2013

[1] J. Mannhart, D. Schlom, *Science* **2010**, *327*, 1607.
[2] A. Ohtomo, H. Y. Hwang, *Nature* **2004**, *427*, 423.
[3] S. Okamoto, A. Millis, *Nature* **2004**, *428*, 630.
[4] J. Chakhalian, J. Freeland, G. Srajer, J. Strempfer, G. Khaliullin, J. Cezar, T. Charlton, R. Dalgliesh, C. Bernhard, G. Cristiani, *Nat. Phys.* **2006**, *2*, 244.
[5] N. Reyren, S. Thiel, A. D. Caviglia, L. F. Kourkoutis, G. Hammerl, C. Richter, C. W. Schneider, T. Kopp, A.-S. Ruetschi, D. Jaccard, M. Gabay, D. A. Muller, J.-M. Triscone, J. Mannhart, *Science* **2007**, *317*, 1196.
[6] F. Y. Bruno, J. Garcia-Barriocanal, M. Varela, N. M. Nemes, P. Thakur, J. C. Cezar, N. B. Brookes, A. Rivera-Calzada, M. Garcia-Hernandez, C. Leon, S. Okamoto, S. J. Pennycook, J. Santamaria, *Phys. Rev. Lett.* **2011**, *106*, 147205.
[7] S. Valencia, C. A. L. Bocher, V. Garcia, X. Moya, R. O. Cherifi, C. Deranlot, K. Bouzehouane, S. Fusil, Z. Zobelli, A. Gloter, N. D. Mathur, A. Gaupp, R. Abrudan, F. Radu, A. Barthelemy, M. Bibes, *Nat. Mater.* **2011**, *10*, 753.
[8] A. Rivera-Calzada, M. Diaz-Guillen, O. Dura, G. Sanchez-Santolino, T. J. Pennycook, R. Schmidt, F. Y. Bruno, J. Garcia-Barriocanal, Z. Sefrioui, N. Nemes, M. Garcia-Hernández, M. Varela, C. Leon, S. T. Pantelides, S. J. Pennycook, J. Santamaria, *Adv. Mater.* **2011**, *23*, 5268.
[9] J. Chakhalian, J. Freeland, H. Habermeier, G. Cristiani, G. Khaliullin, M. van Veenendaal, B. Keimer, *Science* **2007**, *318*, 1114.
[10] J. Garcia-Barriocanal, F. Y. Bruno, A. Rivera-Calzada, Z. Sefrioui, N. M. Nemes, M. Garcia-Hernández, J. Rubio-Zuazo, G. R. Castro, M. Varela, S. J. Pennycook, C. Leon, J. Santamaria, *Adv. Mater.* **2010**, *22*, 627.
[11] P. Moetakef, T. A. Cain, D. G. Ouellette, J. Y. Zhang, D. O. Klenov, A. Jannoti, C. G. Van de Walle, S. Rajan, S. James Allen, S. Stemmer, *Appl. Phys. Lett.* **2011**, *99*, 232116.
[12] S. Yunoki, A. Moreo, E. Dagotto, S. Okamoto, S. Kancharla, A. Fujimori, *Phys. Rev. B* **2007**, *76*, 64532.
[13] G. Alvarez, M. Mayr, A. Moreo, E. Dagotto, *Phys. Rev. B* **2005**, *71*, 014514.
[14] M. Varela, A. R. Lupini, S. J. Pennycook, Z. Sefrioui, J. Santamaria, *Solid-State Electron.* **2003**, *47*, 2245.
[15] S. Smadici, J. Lee, S. Wang, P. Abbamonte, G. Logvenov, A. Gozar, C. Cavellin, I. Bozovic, *Phys. Rev. Lett.* **2009**, *102*, 107004.
[16] M. Nakamura, A. Sawa, H. Sato, H. Akoh, M. Kawasaki, Y. Tokura, *Phys. Rev. B* **2007**, *75*, 155103.
[17] A. Gozar, G. Logvenov, L. F. Kourkoutis, A. Bollinger, L. Giannuzzi, D. Muller, I. Bozovic, *Nature* **2008**, *455*, 782.
[18] Y. Tokura, H. Takagi, S. Uchida, *Nature* **1989**, *337*, 345.
[19] M. Nakamura, A. Sawa, J. Fujioka, M. Kawasaki, Y. Tokura, *Phys. Rev. B* **2010**, *82*, 201101.
[20] H. Wadati, D. Kobayashi, H. Kumigashira, K. Okazaki, T. Mizokawa, A. Fujimori, K. Horiba, M. Oshima, N. Hamada, M. Lippmaa, *Phys. Rev. B* **2005**, *71*, 035108.
[21] M. Imada, A. Fujimori, Y. Tokura, *Rev. Mod. Phys.* **1998**, *70*, 1039.
[22] S. Kivelson, *Phys. B: Condens. Matter* **2002**, *318*, 61.
[23] G. Koster, B. L. Kropman, G. J. H. M. Rijnders, D. H. A. Blank, H. Rogalla, *Appl. Phys. Lett.* **1998**, *73*, 2920.
[24] C. Visani, J. Tornos, N. M. Nemes, M. Rocci, C. Leon, J. Santamaria, S. G. E. te Velthuis, Y. Liu, A. Hoffmann, J. W. Freeland, M. Garcia-Hernandez, M. R. Fitzsimmons, B. J. Kirby, M. Varela, S. J. Pennycook, *Phys. Rev. B* **2011**, *84*, 060405.
[25] N. Browning, M. Chisholm, S. Pennycook, D. Norton, D. Lowndes, *Phys. C: Supercond.* **1993**, *212*, 185.
[26] N. Browning, J. Yuan, L. Brown, *Physica C: Supercond.* **1992**, *202*, 12.
[27] Y. Tokura, N. Nagaosa, *Science* **2000**, *288*, 462.
[28] J. Garcia-Barriocanal, J. C. Cezar, F. Y. Bruno, P. Thakur, N. B. Brookes, C. Utfeld, A. Rivera-Calzada, S. R. Giblin, J. W. Taylor, J. A. Duffy, S. B. Dugdale, T. Nakamura, K. Kodama, C. Leon, S. Okamoto, J. Santamaria, *Nat. Commun.* **2010**, *1*, 82.
[29] S. Okamoto, *Phys. Rev. B* **2010**, *82*, 024427.
[30] C. F. J. Flipse, G. van der Laan, A. L. Johnson, K. Kadowaki, *Phys. Rev. B* **1990**, *42*, 1997.
[31] J. Fink, N. Nücker, E. Pellegrin, H. Romberg, M. Alexander, M. Knupfer, *J. Electron. Spectrosc. Relat. Phenom.* **1994**, *66*, 395.
[32] Y. Tanaka, M. Karppinen, J. M. Chen, R. S. Liu, H. Yamauchi, *J. Solid State Chem.* **2009**, *182*, 1217.
[33] N. Nucker, E. Pellegrin, P. Schweiss, J. Fink, S. L. Molodtsov, C. T. Simmons, G. Kaindl, W. Frentrup, A. Erb, G. Muller-Vogt, *Phys. Rev. B* **1995**, *51*, 8529.
[34] M. Merz, N. Nucker, P. Schweiss, S. Schuppler, C. T. Chen, V. Chakarian, J. Freeland, Y. U. Idzerda, M. Klaser, G. Muller-Vogt, T. Wolf, *Phys. Rev. Lett.* **1998**, *80*, 5192.
[35] M. Karppinen, M. Kotiranta, H. Yamauchi, P. Nachimuthu, R. S. Liu, J. M. Chen, *Phys. Rev. B* **2001**, *63*, 184507.
[36] Y. Onose, Y. Taguchi, K. Ishizaka, Y. Tokura, *Phys. Rev. B* **2004**, *69*, 024504.
[37] M. Huijben, A. Brinkman, G. Koster, G. Rijnders, H. Hilgenkamp, D. H. A. Blank, *Adv. Mater.* **2009**, *21*, 1665.
[38] J. Gauthier, S. Gagne, J. Renaud, M. E. Gosselin, P. Fournier, P. Richard, *Phys. Rev. B* **2007**, *75*, 024424.
[39] J. T. S. Irvine, D. C. Sinclair, A. R. West, *Adv. Mater.* **1990**, *2*, 132.
[40] E. Barsoukov, J. R. Macdonald, *Impedance Spectroscopy: Theory, Experiment, and Applications*, John Wiley and Sons, **2005**.